IL NUOVO CIMENTO **46 C** (2023) 73
DOI 10.1393/ncc/i2023-23073-2

COMMUNICATIONS: SIF Congress 2022

Monte Carlo study of 3D image reconstruction for boron dose distribution in BNCT with CZT-based Compton camera

D. RAMOS[1][2] on behalf of G. M. I. PUGLIESE[1][2], G. IASELLI[1][2], N. PROTTI[3][4], S. ALTIERI[3][4] and C. GONG[5]

([1]) *Università di Bari - Bari, Italy*
([2]) *INFN, Sezione di Bari - Bari, Italy*
([3]) *Università di Pavia - Pavia, Italy*
([4]) *INFN, Sezione di Pavia - Pavia, Italy*
([5]) *Nanjing University of Science and Technologies - Nanjing, China*

received 7 April 2023

Summary. — Boron Neutron Capture Therapy is an innovative and highly selective treatment against cancer. Nowadays *in vivo* boron dosimetry is an important issue to carry out such therapy in clinical environments. In this work, we study the performance of a Compton camera detector based on a 3D CZT crystal for online dosimetry in BNCT using Monte Carlo simulations and the maximum likelihood expectation maximization method for tomography reconstruction.

1. – Introduction

Boron Neutron Capture Therapy (BNCT) is an innovative hadrontherapy with high selectivity over cancer tissue based on the neutron capture reaction $^{10}\mathrm{B}(n,\alpha)^{7}\mathrm{Li}$ [1, 2]. The BNCT is performed by first delivering a specifically designed ^{10}B-enriched molecule to the tumor cell, and by the subsequent irradiation with thermal neutron.

The non-radioactive isotope boron-10 (B10), when irradiated with low energy neutrons (cross section of 3837 barn at 0.025 eV) produces a boron-11 unstable nucleus which converts in approximately 10^{-12} s with a 94% yield, into an α-particle and an excited $^{7}\mathrm{Li}^{*}$ recoil nucleus. The excited lithium nucleus then decays emitting a prompt gamma ray of 478 keV. The reaction has a positive Q-value of 2.78 MeV and the products have high linear energy transfer (LET) that deposits the energy within a range $<10\,\mu$m, making the energy transfer (up to 83% on average) in the cancer cell possible. The prompt gamma emission and short range of the reaction products guarantee the spatial correlation.

A topic of primary importance in BNCT dosimetry is the measurement of the dose given to the patient during treatments. Nowadays the boron dosimetry is carried out through indirect and separated measurements of B10 concentration by several blood

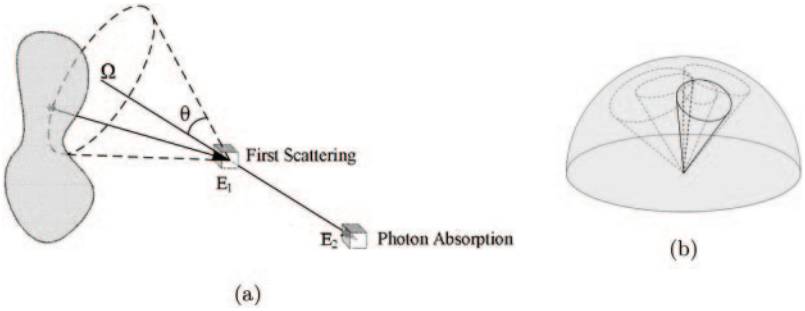

Fig. 1. – Compton camera imaging schema. (a) Compton camera principle, (b) overlapped cones in the most likely position of the source.

tests (before, meanwhile and after irradiation), and local thermal neutron flux estimations made by treatment planning systems. This procedure leads to large uncertainties in clinical dosimetry. Therefore a possible protocol based on the measurement of the prompt gamma-ray of 478 keV becomes significant to be able to reconstruct *in vivo* the spatial distribution of the dose in the area of interest. To such aim, we will investigate imaging algorithm methods such as computed tomography using "Compton Camera techniques" [3].

In this approach, a 3D sensor capable to determine, in addition to the energy of the emitted photon, also its position, is needed. In this contest a high-resolution 3D cadmium-zinc-telluride (CZT) drift strip detector has been proposed, able to perform room-temperature measurements of photon energy, timing and 3D positioning up to the MeV region. Recently, very preliminary results of the spectroscopic capabilities of such spectro-imager has been reported in the energy range of interest of BNCT [4].

In this work, we have used Monte Carlo simulations and the Maximum Likelihood Expectation Maximization (MLEM) iterative method to study the 3D CZT Compton camera detector performance within the BNCT framework.

2. – Compton imaging

The Compton camera method to reconstruct images is based on Compton kinematics to find the origin of the detected gamma ray. Typically the camera is constituted by two distinct detectors: the first one known as scatterer and having the function of promoting the Compton interaction of the incident gamma; the second one known as the absorber to stop, by photoelectric effect, the scattered photon. Generally the two detectors are separated thus delimiting a small working solid angle of the Compton Camera. The possibility of having a double layer detector acting at the same time as scatterer as well as absorber improves the detection efficiency of the system [5].

The hits in the two detectors and the measured absorbed energies are used to calculate the scattering angle, as is shown in fig. 1(a), and the most likely origin spot by superposition of different Compton cones, as represented in fig. 1(b). In the present study, we take into account only the events in which a photon has Compton scattering and photoabsorption in two different detector planes. Such events are called as *true events*. In this sense, the development of a 3D spectro imager allows the 4π Compton Imaging solving the Compton kinematic equation. Then, knowing the gamma incident energy, the measurement of the absorbed energy fully determines the Compton scattering angle

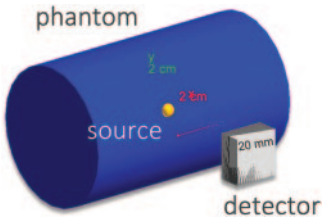

Fig. 2. – Simulated set-up on GEANT4.

according to

$$\cos\theta = 1 - m_e c^2 \left(\frac{1}{E_2} - \frac{1}{E_\gamma}\right); \tag{1}$$
$$E_\gamma = E_1 + E_2,$$

where E_γ is the incident photon energy and E_1 and E_2 are the energies deposited in the scatter layer and absorption layer, respectively.

The image revealed directly by the detector using Compton kinematics will be referred as "back-projection image" in what follows.

3. – Monte Carlo simulation and image reconstruction

The Monte Carlo simulations were carried out using GEANT4 framework [6]. The code was exploited in the 10.7 software version. In order to implement the most accurate low-energy models, the Electromagnetic Standard Option 4 (emstandard_opt4) physics list package was used.

The simulated setup was composed by a solid cylinder phantom made of air or soft tissue (both defined in GEANT4 material database) with 30 mm radius and 100 mm height, and a Compton camera with two adjacent CZT crystal layers with dimension $20 \times 20 \times 5\,\mathrm{mm}^3$ and $5.78\,\mathrm{g\ cm}^{-3}$ density each. The camera was situated in the Z-axis as shown fig. 2. The distance between the detector and the gamma source (yellow mark) in the figure can be varied.

The gamma source was set with an energy of 478 keV, and a single spherical geometry of 10 mm radius was used since it is a closer model of a real tumor.

The source was centered in the coordinates system origin. Since in realistic BNCT treatments boron can also load healthy tissue in a given proportion, we define the tumor-to-healthy boron concentration ratio T as the boron concentration between tumor tissue and healthy tissue. Additional random gammas were generated in the phantom with vertex positions outside the source with given T values.

The hits position (without taking into account the uncertainties introduced by the intrinsic space resolution of the detector), and the energy deposited of *true events* were used to reconstruct the back-projection images.

Those images were set in gray-scale, normalized to a maximum pixel intensity, and provided in .csv format structured in 8 fields: pixel intensity; x, y, and z pixel position; i, j, and k pixel indexes, and binary source which corresponds to 0 or 1 related to the simulated source.

The list mode MLEM method was chosen for the tomography images reconstruction. This method, described in [7] and [8], has been proved already to be suitable for Compton imaging. The iterative algorithm is given by

$$\lambda_j^{(n+1)} = \frac{\lambda_j^{(n)}}{s_j} \sum_{i=1}^{M} \frac{t_{ij}}{\sum_k t_{ik} \lambda_k^{(n)}}, \tag{2}$$

where $\lambda_j^{(n)}$ is the value of pixel j at iteration n, s_j is the sensitivity matrix representing the probability of a gamma ray emitted from pixel j to be detected, M is the number of measured events and the system matrix t_{ij} is the probability of a gamma ray emitted from pixel j to be detected by the measurement with index i.

The algorithm used for the calculation was the GPU-based image reconstruction code UCT-MLEM [9]. The images were reconstructed in a 100^3 matrix pixels grid in the space volume from -60 mm to 60 mm for each axis (cube pixel image with 1.2 mm side) covering the entire phantom.

Since the images are digital, the most immediate way to quantify goodness is to establish how many pixels belong to the reconstructed regions. It was possible to identify, within the image matrix, the pixel intensity, and its quantification.

The reconstructed images were binarized: the number of pixels having intensity "1" belonging to the overlapping region between the real image and the reconstructed one represents the number of *true positive* (TP); the number of pixels belonging to the image reconstructed but not to the real source represents the number of *false positive* (FP); finally, the number of pixels belonging to the real source but not present in the reconstructed image represents the number of *false negative* (FN). For the result discussion we define:

$$Accuracy = \frac{TP}{TP + FP}, \tag{3}$$

$$Sensitivity = \frac{TP}{TP + FN}. \tag{4}$$

4. – Results and discussion

The source was analyzed in the following situations: 1) in air or tissue to study the dispersion in the phantom itself; 2) in tissue with different T values ($T = 5.0$, 2.0) and the detector at different distances (30.0, 60.0, 100.0 and 200.0 mm). From clinical studies it is well known that for effective treatment with BNCT, the therapeutic ratio should be 3:1 or more [10]; the case $T = 2.0$ has been analyzed as an extreme case.

4˙1. *Reconstruction algorithm validation.* – In order to check the performance of the MLEM algorithm in the BNCT framework with Compton Camera, 250 iterations were carried out in air with the detector 60 mm apart from the source. The spherical volume was reconstructed as shown in fig. 3. When the iteration number is as high as 250, the algorithm develops a sort of granularity in the XY-image (see fig. 3). It is found that 50 iterations are enough to obtain an image with acceptable resolution according to the algorithm convergence, and avoid the granularity issue.

Figure 4 shows the XY-plane tomography image for the source in tissue after 50 iterations. Comparing the results in those two cases (air *vs.* tissue) it is possible to conclude that the dispersion effect due to the tissue is not appreciable.

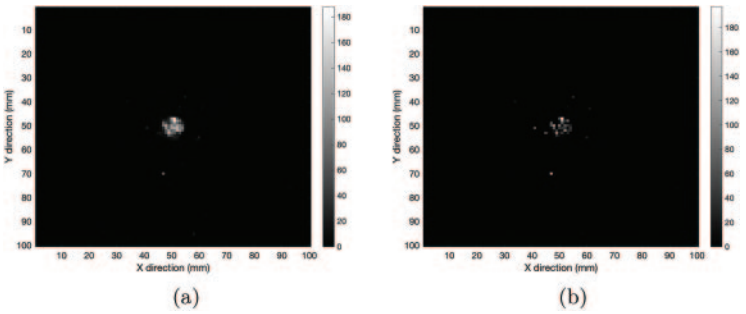

Fig. 3. – XY-plane tomography images of the spherical distribution in air after (a) 50, and (b) 250 iterations.

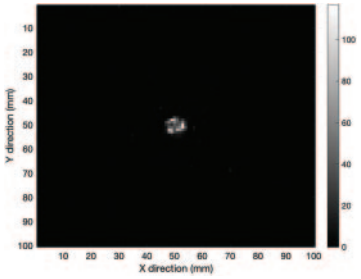

Fig. 4. – XY-plane tomography image for a spherical source in tissue after 50 iterations.

In the case of tissue presence, the X and Y axis profiles were also analyzed and are reported in fig. 5.

Accuracy and sensitivity values are reported in table I, and confirm the statements that 50 iterations are enough to have a good reconstruction in balance with the computational calculation time, and the introduction of the phantom itself does not introduce dispersion in the reconstruction.

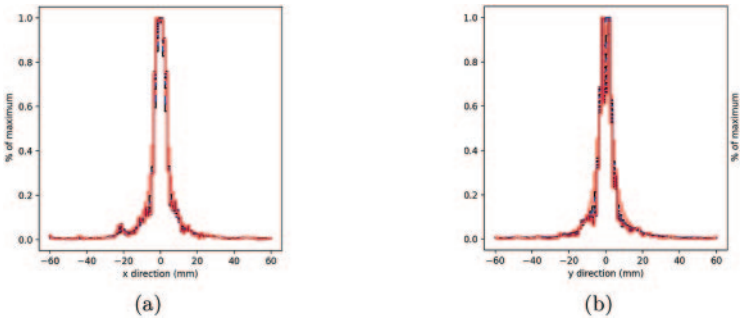

Fig. 5. – Spherical source normalized profiles in tissue. For each curve, 10 more iterations are added to the algorithm till 250 iterations are reached. (a) X-axis, (b) Y-axis reconstruction

TABLE I. – *Reconstruction parameters for spherical configuration.*

Phantom/iterations	Accuracy	Sensitivity
Air, $i = 50$	97.67%	52.5%
Air, $i = 250$	86.95%	25.0%
Tissue, $i = 50$	100.0%	43.75%

4˙2. *Stretching along Z-axis.* – Is also interesting to study the XZ tomography image. Figure 6 shows the XZ-plane tomography image for the source in tissue after 250 iterations fig. 6(a), and the reconstruction profiles along the Z-direction fig. 6(b). It is evident even with a large number of iterations the presence of a stretching effect along the Z-axis.

Previous studies have already demonstrated that this stretching effect arises at larger Compton scattering angles (θ) [11]. Then, to investigate the stretching behavior, measures with the detector at distance values in the range from 30 to 100 mm were performed. The Z-axis profiles after 250 iterations were fitted with Gaussian distributions. Figure 7 shows the fitted sigmas *vs.* the detector distance values; therefore longer stretching is associated with larger distances.

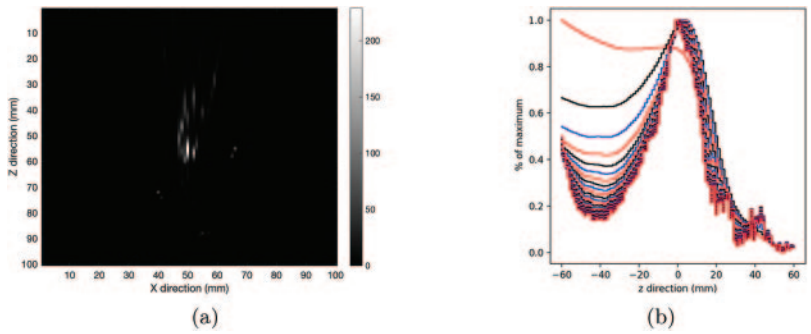

Fig. 6. – (a) XZ-plane tomography image; (b) Z-axis profiles reconstruction for spherical source in tissue after 250 iterations.

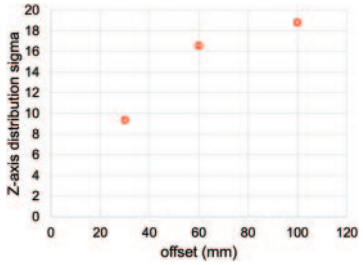

Fig. 7. – Gaussian distribution sigmas of Z-axis profiles for the spherical source at different detector distances.

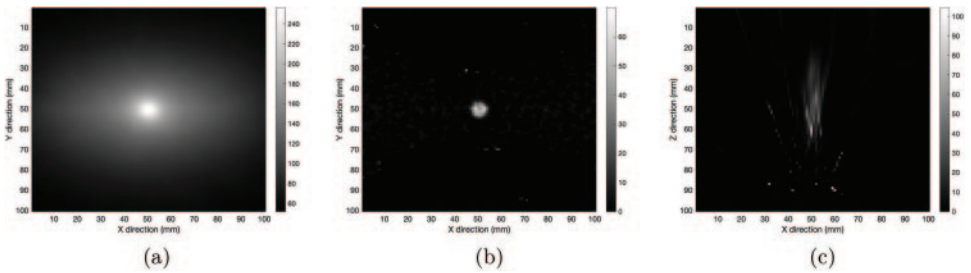

(a) (b) (c)

Fig. 8. – Spherical source with therapeutic ratio $T = 5.0$ and detector distance 60 mm. (a) XY-plane back-projection; (b) XY-plane tomography after 50 iterations, and (c) XZ-plane tomography after 250 iterations.

4˙3. *Dependence by boron concentration ratio.* – The boron concentration ratio dependence was investigated with the detector 60 mm apart from the source, and values $T = 5.0$ and 2.0. Results are shown in figs. 8 and 9, respectively. Looking at the figures, it is evident the noise increase when the boron-10 concentration increases in the healthy tissue. This result confirms the expected experimental behavior, since at lower T values there is more energy deposited in the healthy tissue with respect to the tumor region, which enhances the image background in the reconstruction process. Nonetheless, the source was reconstructed at least in the xy-plane even with the lowest concentration under study.

5. – Conclusions

The reconstruction of Compton gammas rays tomography images in the BNCT treatment was studied by the Maximum Likelihood Expectation Maximization. The spherical gamma source configuration was analyzed in several experimental setups. Preliminary evidence that this approach would be capable to evaluate the boron dose inside the patient are reported. The image reconstruction algorithm does not suffer from dispersion effects of the healthy tissue. The study of Z-axis profiles opens the possibility to estimate the distance between the source and the detector through the calculation of the sigma stretching. In addition, by studying the boron concentration ratio dependence was found that the algorithm and the simulated detector are sensible to different T values.

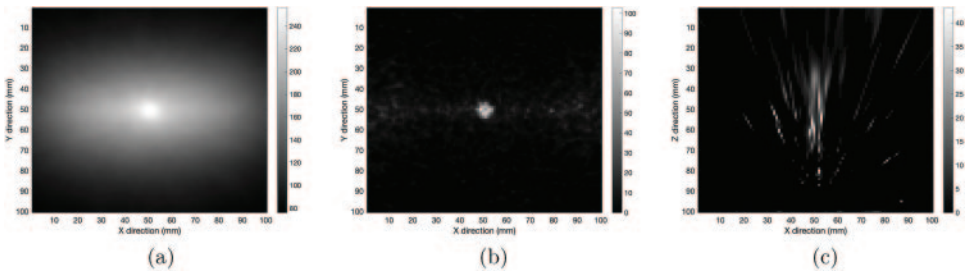

(a) (b) (c)

Fig. 9. – Spherical source with therapeutic ratio $T = 2.0$ and detector distance 60 mm. (a) XY-plane back-projection; (b) XY-plane tomography with 50 iterations, and (c) XZ-plane tomography with 250 iterations.

REFERENCES

[1] Malouff T. D., Seneviratne D. S., Ebner D. K. *et al.*, *Front. Oncol.*, **11** (2021) 601820.

[2] Dymova M., Taskaev S., Richter V. and Kuligina E., *Cancer Commun.*, **40** (2020) 406.

[3] Lee T., Lee H. and Lee W., *Nucl. Instrum. Methods Phys. Res. A*, **798** (2015) 135.

[4] Abbene L., Principato F., Buttacavoli A. *et al.*, *Sensors*, **22** (2022) 1502.

[5] Muñoz E., Barrio J., Etxebeste A. *et al.*, *Phys. Med. Biol.*, **62** (2017) 7321.

[6] Agostinelli S., Allison J., Amako K. *et al.*, *Nucl. Instrum. Methods Phys. Res. A*, **506** (2003) 250.

[7] Hebert T., Leahy R. and Singh M., *J. Opt. Soc. Am. A*, **7** (1990) 1305.

[8] Wilderman S., Clinthorne N., Fessler J. *et al.*, *List-mode maximum likelihood reconstruction of compton scatter camera images in nuclear medicine* in *proceedings of 1998 IEEE Nuclear Science Symposium Conference Record. 1998 IEEE Nuclear Science Symposium and Medical Imaging Conference (Cat. No.98CH36255)*, Vol. **3** (IEEE) 1998, pp. 1716–1720.

[9] Leigh M. and Peterson S., *UCT-MLEM - A MLEM Compton camera image reconstruction code* (2018) `https://github.com/mattcleigh/Compton_MLEM`.

[10] Skwierawska D., Lápez-Valverde J. A., Balcerzyk M. *et al.*, *Cancers*, **14** (2022) 2865.

[11] Cong F., Tamura Y., Shimazoe K. *et al.*, *Nucl. Instrum. Methods Phys. Res. A*, **953** (2020) 163108.